Biogeochemistry (2011) 103:263–279
DOI 10.1007/s10533-010-9461-2

Effects of hyper-enriched reactive Fe on sulfidisation in a tidally inundated acid sulfate soil wetland

Annabelle F. Keene · Scott G. Johnston · Richard T. Bush · Leigh A. Sullivan · Edward D. Burton · Angus E. McElnea · Colin R. Ahern · Bernard Powell

Received: 18 October 2009 / Accepted: 29 April 2010 / Published online: 14 May 2010

Abstract Solid phase Fe and S fractions were examined in an acid sulfate soil (ASS) wetland undergoing remediation via tidal inundation. Considerable diagenetic enrichment of reactive Fe(III) oxides (HCl- and dithionite-extractable) occurred near the soil surface (0–0.05 m depth), where extremely large concentrations up to 3534 μmol/g accounted for ~90% of the total Fe pool. This major source of reactive Fe exerts a substantial influence on S cycling and the formation, speciation and transformation of reduced inorganic S (RIS) in tidally inundated ASS. Under these geochemical conditions, acid volatile sulfide (AVS; up to 57 μmol/g) and elemental sulfur (S^0; up to 41 μmol/g) were the dominant fractions of RIS in near surface soils. AVS–S to pyrite–S ratios exceeded 2.9 near the surface, indicating that abundant reactive Fe favoured the accumulation of AVS minerals and S^0 over pyrite. This is supported by the significant correlation of poorly crystalline Fe with AVS–S and S^0–S contents ($r = 0.83$ and $r = 0.85$, respectively, $P < 0.01$). XANES spectroscopy provided direct evidence for the presence of a greigite-like phase in AVS–S measured by chemical extraction. While the abundant reactive Fe may limit the transformation of AVS minerals and S^0 to pyrite during early diagenesis (~5 years), continued sulfidisation over longer time scales is likely to eventually lead to enhanced sequestration of S within pyrite (with a predicted 8% pyrite by mass). These findings provide an important understanding of sulfidisation processes occurring in reactive Fe-enriched, tidally inundated ASS landscapes.

Keywords Acid sulfate soil · Reactive iron · Reduced inorganic sulfur · Sulfidisation · Tidal inundation · Wetland

Abbreviations

ASS	Acid sulfate soil
AVS	Acid volatile sulfide
CRS	Chromium-reducible sulfur
DOP	Degree of pyritisation
DOS	Degree of sulfidisation
RIS	Reduced inorganic sulfur
XANES	X-ray absorption near-edge structure

A. F. Keene (✉) · S. G. Johnston · R. T. Bush · L. A. Sullivan · E. D. Burton
Southern Cross GeoScience, Southern Cross University, PO Box 157, Lismore, NSW 2480, Australia
e-mail: annabelle.keene@scu.edu.au

A. E. McElnea · C. R. Ahern · B. Powell
Department of Environment and Resource Management, 80 Meiers Road, Indooroopilly, QLD 4068, Australia

Introduction

Cycling of Fe and S is a key process in the biogeochemistry of intertidal estuarine sediments (e.g., Giblin and Howarth 1984; Canfield 1989;

Luther et al. 1991; Kostka and Luther 1995; Morse and Rickard 2004). In these sedimentary environments, bioauthigenic pyrite (FeS_2) is an important iron sulfide mineral component and a major sink for reduced S. Its formation via the process of sulfidisation has been studied extensively (e.g., Berner 1970; Lord and Church 1983; Howarth and Jørgensen 1984; Boesen and Postma 1988). Drainage of sulfide-rich, estuarine materials is known to cause rapid oxidation of pyrite, leading to severe acidification and the development of acid sulfate soils (ASS) (van Breemen 1973; Dent 1986).

The mobilisation of acidic solutes and trace metals from drained ASS landscapes can degrade the water quality of adjacent aquatic habitats and is a widely recognised, internationally significant environmental problem (e.g., Sammut et al. 1996; Portnoy and Giblin 1997; Sundström et al. 2002; Macdonald et al. 2004; Lax 2005; Fältmarsch et al. 2008). An innovative approach to remediating ASS landscapes is to restore tidal inundation (Powell and Martens 2005; Johnston et al. 2009a). Tidal inundation radically alters the geochemical conditions of soils and sediments, promoting bacterially-mediated reduction of Fe(III) and SO_4^{2-}. Such reductive transformations consume acidity, generate alkalinity and encourage the reformation of iron sulfide minerals such as pyrite (Hicks et al. 2003; Johnston et al. 2009b).

In drained ASS, some of the Fe released from pyrite oxidation typically forms Fe(III) minerals, including goethite (α-FeOOH), jarosite ($KFe_3(SO_4)_2(OH)_6$) and schwertmannite ($Fe_8O_8(OH)_6SO_4$) (e.g., Sullivan and Bush 2004). Re-establishing tidal inundation in ASS can cause reductive dissolution of these minerals within the soil profile and lead to substantial enrichment of the reactive Fe fraction near the soil surface (Johnston et al. 2009b). Reactive Fe is a key component in the formation of iron sulfide minerals, and is defined as that Fe which readily reacts with dissolved sulfides (Berner 1970; Canfield 1989; Canfield et al. 1992). For example, the oxidation of H_2S by Fe(III) (oxyhydr)oxides such as goethite (Rickard 1974; Pyzik and Sommer 1981) can be described by the reaction:

$$2\alpha\text{-FeOOH} + 3H_2S \rightarrow 2FeS + S^0 + 4H_2O \quad (1)$$

The abundance of solid phase Fe and its reactivity toward sulfides is a major factor influencing the formation of reduced inorganic S (RIS) species, and hence the degree of pyritisation (DOP), in coastal marine and estuarine sediments.

In addition to pyrite, other RIS species formed in sulfide-rich sedimentary environments include elemental S (S^0) and acid volatile sulfides (AVS). AVS comprises porewater sulfides (including dissolved Fe(II)–sulfide complexes and aqueous FeS clusters) and a suite of metastable iron sulfides including the minerals mackinawite (FeS) and greigite (Fe_3S_4) (Cornwell and Morse 1987; Morse and Rickard 2004; Rickard and Morse 2005). AVS and S^0 are generally a minor fraction of RIS in coastal marine and estuarine sediments (Giblin and Wieder 1992; Morse and Rickard 2004), but are found at appreciable proportions of RIS in organic, sulfide-rich materials from ASS landscapes (Bush et al. 2004; Macdonald et al. 2004; Burton et al. 2006b; Boman et al. 2008, 2010).

The concentration and distribution of RIS in marine and estuarine sediments is primarily controlled by the availability of reactive Fe. Abundant reactive Fe can sequester most of the sulfides (e.g., H_2S) in iron sulfides and constrain the concentration of dissolved sulfide in porewaters (Canfield 1989; Canfield et al. 1992). This promotes the formation and accumulation of FeS, as a lack of dissolved sulfide to react with FeS retards its subsequent transformation to pyrite (Rickard and Morse 2005). Fe(III) reduction is energetically favoured over SO_4^{2-} reduction (Lovely and Phillips 1987; Postma and Jacobsen 1996; Burton et al. 2007, 2008a), and this can lead to the formation of FeS and S^0 via rapid oxidation of H_2S by reactive Fe(III) minerals (see Eq. 1, Yao and Millero 1996; Poulton 2003). Although mackinawite and greigite are not direct precursors to pyrite (Rickard and Morse 2005), these metastable AVS minerals provide a solid phase source of dissolved sulfide for pyrite formation in marine and estuarine sediments. Pyrite can form with the sequestration of reduced S species in partially oxic to anoxic environments via the polysulfide pathway (Rickard 1975), according to the overall defining equation (Berner 1970):

$$FeS + S^0 \rightarrow FeS_2 \quad (2)$$

Alternatively, FeS can be transformed to pyrite through the H_2S mechanism favoured under strictly

anoxic conditions (Rickard 1997), according to the overall reaction:

$$FeS + H_2S \rightarrow FeS_2 + H_2 \quad (3)$$

Whilst numerous studies have examined the coupled cycling of solid phase Fe and S in coastal marine and estuarine sediments (e.g., Canfield et al. 1992; Holmer et al. 1994; Kostka and Luther 1995), this study provides the first examination of sulfidisation in tidally inundated ASS wetlands. The exceptional enrichment of reactive Fe in this sedimentary environment provides an ideal opportunity to investigate the composition and transformation of RIS species in the field where Fe is not limiting.

In this study, we quantify the in situ partitioning of solid phase Fe and S following tidal inundation of a previously drained ASS wetland. Our objective is to examine the key geochemical role of enriched reactive Fe for RIS speciation. In addition, we consider the short and long term implications of these transformations for remediation of coastal ASS landscapes by tidal inundation.

Materials and methods

Study area

The study area was located in a Holocene sedimentary coastal plain at East Trinity near Cairns in northeastern Australia (145°48′ E, 16°56′ S; Fig. 1a). The East Trinity field site covers an area of 940 ha on the eastern side of Trinity Inlet and is dissected by Hills Creek which drains the granitic ranges to the east. It experiences a tropical monsoonal climate with summer-dominant rainfall (mean annual rainfall of 2015 mm at Cairns Aero, Station No. 31011, Bureau of Meteorology 2010) and a maximum tidal range in Trinity Inlet of around 3.2 m. Sediments are dominated by estuarine muds underlain by transgressive mangrove muds and marine muds deposited during Holocene chenier plain evolution (Smith et al. 2003).

Prior to extensive drainage and clearing of vegetation for agriculture, the study site contained large areas of tidal estuarine wetlands, including mangrove and saltmarsh communities. Drainage was facilitated by construction in the early 1970s of a 5 km sea wall incorporating tide-excluding floodgates on the major creeks. Estuarine wetlands and creeks inside the sea wall were isolated from tidal inundation, causing oxidation of pyrite-rich (~2% g/g) estuarine sediments and subsequent development of severely acidic soils (Hicks et al. 1999). The Queensland Government has made a multi-million dollar investment to enable rehabilitation of the East Trinity site. Various parts of the site have undergone remediation from 2001, which consisted of the reintroduction of regular tidal inundation to the previously drained ASS (Powell and Martens 2005; Johnston et al. 2009a). The remediation strategy for East Trinity is summarised in Powell and Martens (2005), and the resulting pedogenic changes to degraded ASS of the Firewood Creek sub-catchment are described in Johnston et al. (2009b).

For this study, two physiographic settings were located within Firewood Creek sub-catchment (Fig. 1). Sampling sites were selected to represent an intertidal ASS mudflat, with one vegetated (M) and one unvegetated (MF). Both ASS settings were located approximately 1.1 km upstream from the tidal floodgates and have experienced regular but attenuated tidal inundation for the preceding 5 years (i.e., since 2003). M was situated within a narrow zone of young (<5 years), recolonising *Avicennia* mangroves. MF consisted of an extensive bare mudflat adjoining the sea wall. An additional physiographic setting was located immediately outside the East Trinity remediation site along Trinity Inlet (Fig. 1). This reference site was selected to represent a natural, undrained mangrove wetland (TI) and based on proximity to the other sampling sites. TI experienced a natural tidal range representative of undrained conditions, and consisted of an intertidal *Rhizophora*-dominated mangrove forest, 360 m from the seaward fringe of mangroves and unaffected by previous drainage of ASS at the Firewood Creek site.

Soil and sediment collection and handling

Three duplicate core profiles were collected within each physiographic setting in March 2008 using a Russian D-section corer (internal diameter 0.075 m, length 0.75 m). Soils and sediments were rapidly sectioned into specified depth intervals (from 0 to 0.05, 0.05 to 0.15 m depth, and thereafter in 0.10 m increments) below ground level (bgl) for analysis of the solid fraction. Sampling at TI was confined to near surface materials (to 0.15 m depth) and

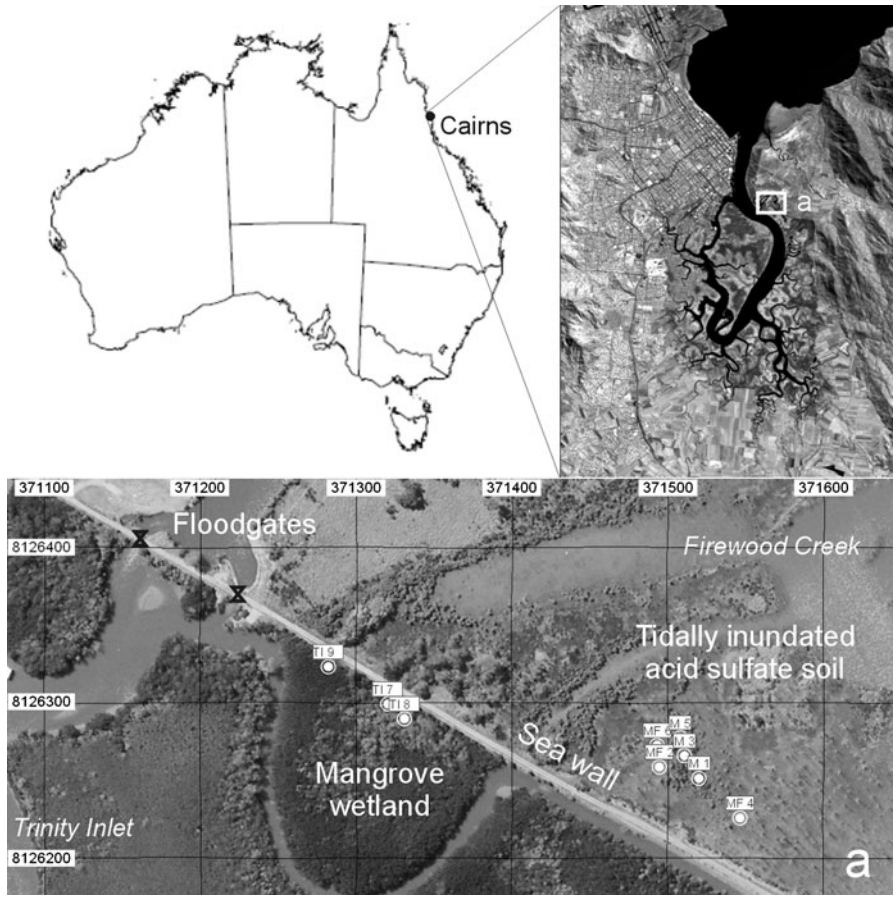

Fig. 1 Location of the study area at East Trinity near Cairns in northeastern Australia. *Inset a* shows Firewood Creek study site and designated sampling points: vegetated ASS mudflat (M), unvegetated ASS mudflat (MF) and Trinity Inlet mangrove wetland (TI). Universal Transverse Mercator coordinates in Easting and Northing

undertaken for comparative purposes. Data points shown here represent the average of each depth interval. Field measurements of pH (pH_F) and Eh (Eh_F) were made immediately on each undisturbed core by direct probe insertion using calibrated Intermediate Junction Ag/AgCl combination pH and ORP electrodes with a saturated KCl reference solution. Eh measurements were corrected to the Standard Hydrogen Electrode (SHE). Duplicate samples from the equivalent depth intervals were bulked and placed into air-tight, sealable polyethylene bags, completely filled with material (i.e., no enclosed air). All soil and sediment samples were stored frozen until analysis to minimise possible oxidation of reduced species.

Solid phase chemical analyses

In the laboratory, frozen samples were thawed under N_2 and homogenised with a spatula for analysis of the solid fraction. Gravimetric moisture content (θ_g) was determined by oven-drying sub-samples at 105°C until a constant mass (Rayment and Higginson 1992). General characterisation of soils and sediments was undertaken on oven-dry materials. Operationally defined solid phase reactive Fe and RIS fractions were extracted sequentially from moist soils and sediments. All sequential extractions were undertaken in triplicate on 1–2 g sub-samples (error bars refer to triplicate extractions from each depth interval). The sequential chemical extraction methods used in this study and the operationally defined reactive Fe and RIS fractions differentiated by each extraction are provided in Table 1.

All laboratory equipment used during collection and analysis of soils and sediments was previously immersed in 30% HCl for at least 24 h and then rinsed repeatedly with Milli-Q water. Reagents were analytical grade and all reagent solutions were prepared with Milli-Q water. Deoxygenated solutions

Table 1 Sequential chemical extractions used to differentiate the operationally defined Fe or S fractions of soils and sediments

Extractant	Concentration	Volume (ml)	Time (h)	Fe or S mineral	Fraction defined	Procedure
Reactive Fe speciation						
HCl	1.0 M	30	1.0	Ferrihydrite, schwertmannite, lepidocrocite, AVS	Poorly crystalline Fe (minus AVS–Fe)	Burton et al. (2006a)
↓						
Dithionite	50 g/l	40	4.0	Goethite, hematite, magnetite	Crystalline Fe	Kostka and Luther (1994)
RIS speciation						
HCl	6.0 M	40	18	Mackinawite, greigite	AVS–S	Hsieh et al. (2002)
↓						
Toluene		10	16	Elemental S	S^0–S	Burton et al. (2009)
↓						
Acidic Cr(II)	500 g/l	12	48	Pyrite	FeS_2–S	Burton et al. (2008a, b)

Pyrite and AVS measured as S and converted to Fe equivalents using a 2:1 and 1:1 S to Fe ratio, respectively

were prepared by purging with N_2 for at least 0.5 h. All solid phase results are presented on a dry mass basis (except where otherwise noted).

Reactive Fe speciation

To determine HCl-extractable Fe, 30 ml of 1 M HCl was added to the moist sediment and mixed on an orbital shaker at 125 rpm for 1 h then centrifuged at 3000 rpm for 10 min, based on the cold extraction procedures detailed in Huerta-Díaz and Morse (1990), Leventhal and Taylor (1990), Wallmann et al. (1993), Kostka and Luther (1994), Raiswell et al. (1994) and Burton et al. (2006a). HCl-extractable Fe(II) and total Fe concentrations were determined by the 1,10-phenanthroline method using spectrophotometry, with the addition of hydroxylammonium chloride for total Fe (APHA-AWWA-WEF 2005). HCl-extractable Fe(III) was calculated by the difference between HCl-extractable total Fe and HCl-extractable Fe(II).

To determine dithionite-extractable Fe, 40 ml of 0.35 M glacial acetic acid/0.2 M sodium citrate and 2 g sodium dithionite were added to the remaining sediment and mixed on an orbital shaker at 125 rpm for 4 h then centrifuged at 3000 rpm for 10 min, based on the procedure detailed in Kostka and Luther (1994) and Raiswell et al. (1994). Dithionite-extractable Fe was determined by the 1,10-phenanthroline method using spectrophotometry (APHA-AWWA-WEF 2005).

The cold, dilute HCl and dithionite extractions are selective for reactive, poorly crystalline Fe (oxyhydr)oxides and readily reducible, crystalline Fe(III) oxides, respectively (Canfield 1989; Canfield et al. 1992; Wallmann et al. 1993; Kostka and Luther 1994; Raiswell et al. 1994). HCl extractions effectively leach poorly crystalline Fe (oxyhydr) oxide fractions including ferrihydrite and lepidocrocite, as well as iron monosulfides (Wallmann et al. 1993; Kostka and Luther 1994; Raiswell et al. 1994). Dithionite extractions effectively leach Fe from more crystalline Fe(III) minerals including goethite, hematite and magnetite, but not from clay minerals (Canfield et al. 1992; Kostka and Luther 1994; Raiswell et al. 1994). Hence, the poorly crystalline Fe fraction is operationally defined as the HCl-extractable total Fe minus the Fe associated with AVS (i.e., iron monosulfides), and the crystalline Fe fraction is operationally defined as that soluble in dithionite (Table 1). Together, these fractions provide an estimate of the reactive (non-sulfidic) Fe pool present in the soils and sediments. AVS–Fe and pyrite–Fe accounted for the Fe associated with AVS and pyrite, and were estimated from the concentration of AVS–S and pyrite–S, assuming a ratio of S to Fe of 1:1 and 2:1, respectively. Unreactive Fe (or residual Fe) is Fe

sheet silicates found by the difference between the total Fe content and the sum of other defined Fe fractions.

RIS speciation

To determine AVS–S, 10 ml of 6 M HCl/0.1 M $C_6H_8O_6$ was added to the moist sediment and mixed on an orbital shaker at 125 rpm for 18 h (Table 1). The evolved H_2S was trapped in 5 ml 3% $Zn(CH_3COO)_2{\cdot}2H_2O$ in 2 M NaOH, based on the cold diffusion procedure detailed in Hsieh et al. (2002) using a modified apparatus described by Burton et al. (2007). This method uses ascorbic acid to prevent interferences from Fe(III) and extraction of pyrite–S (Burton et al. 2009). The suspension was then centrifuged at 3000 rpm for 10 min, the sediment retained and the aqueous supernatant discarded. AVS–S concentration was determined in Zn acetate traps by iodometric titration (APHA-AWWA-WEF 2005). AVS–S provided an estimate of the reactive sulfide pool (Morse and Rickard 2004; Rickard and Morse 2005).

To determine S^0–S, 10 ml of toluene and 10 ml of Milli-Q water were added to the remaining sediment and mixed on an orbital shaker at 125 rpm for 16 h then centrifuged at 3000 rpm for 10 min (Table 1), based on the procedure detailed in Burton et al. (2009). S^0–S concentration was determined by the cold cyanolysis method using spectrophotometry (Bartlett and Skoog 1954). The remaining sediment was washed three times with 25 ml acetone and once with 20 ml ethanol to remove residual S^0 prior to the subsequent extraction step.

To determine chromium-reducible S (CRS), 12 ml of acidic Cr(II) solution was added to the sediment and mixed on an orbital shaker at 150 rpm for 48 h with periodic sonification using an ultrasonic bath (Table 1). The evolved H_2S was trapped in 5 ml 3% $Zn(CH_3COO)_2{\cdot}2H_2O$ in 2 M NaOH, based on the diffusion procedure detailed in Burton et al. (2008b). The CRS extraction is a widely used proxy for pyrite (e.g., Canfield et al. 1986; Boman et al. 2010). Pyrite–S concentration was similarly determined in Zn acetate traps by iodometric titration (APHA-AWWA-WEF 2005).

General analytical procedures

A portion of soil and sediment samples were dried for general chemical analysis in a fan-forced, air-extracting oven at 85°C for at least 24 h and ground using a mortar and pestle to pass a 2 mm sieve. Aqueous extractions were undertaken in duplicate on 2 g oven-dry soils and sediments using a 1:5 soil to water ratio (Rayment and Higginson 1992). The aqueous extract was passed through a 0.45 μm syringe-driven filter and water-soluble alkali cations (Na^+, K^+, Ca^{2+} and Mg^{2+}) were determined by Inductively Coupled Plasma-Optical Emission Spectrometry (ICP-OES) using a Perkin-Elmer DV4300 instrument. Water-soluble SO_4^{2-} was determined turbidimetrically using spectrophotometry, and water soluble Cl^- by flow injection analysis (FIA) using a Lachat QuikChem 8000 instrument (APHA-AWWA-WEF 2005). Total C was determined gravimetrically on oven-dry materials using a LECO CNS-2000 Carbon, Nitrogen and Sulfur Analyzer. Near-total Fe and S were determined on oven-dry materials by hot acidic digestion (1:1 HNO_3:HCl, 95°C) for 1 h using a 1:100 soil to solution ratio and measured by Inductively Coupled Plasma-Mass Spectrometry (ICP-MS) using a Perkin-Elmer ELAN-DRCe instrument.

X-ray absorption near-edge structure spectroscopy

RIS speciation in three selected samples (M: 0–0.05 m depth; MF: 0–0.05 m and 0.35–0.45 m depth) was also determined by S K-edge XANES spectroscopy. It is well established that the AVS–S extraction method recovers AVS minerals mackinawite and greigite as well as dissolved sulfides and FeS clusters and nanoparticles (Hsieh et al. 2002; Morse and Rickard 2004; Rickard and Morse 2005). The XANES data were collected on the bending magnet beam-line 16A at the National Synchrotron Radiation Research Centre (NSRRC) in Hsinchu, Taiwan. Mineral standards and soil samples for XANES were transported from Australia to Taiwan frozen under N_2 and stored in this way until analysis. Samples were mounted into 6 μm S-free Mylar film pouches (to minimize atmospheric exposure) prior to XANES analysis under an inert (He) atmosphere at ambient temperature. The X-ray energy resolution was maintained by a fully tuned Si(111) double

crystal monochromator, with the energy calibrated to the maximum of the first feature of $NaS_2O_3 \cdot 5H_2O$ at 2472.02 eV. X-ray fluorescence data were collected using a Lytle detector at ambient temperature under a He atmosphere.

Prior to XANES spectral analysis, the pre-edge background was subtracted and the edge jump was normalized to unity with the PySpline software package (Tenderholt et al. 2006). Qualitative S speciation was determined by comparison of the XANES peak energies for a given soil sample spectrum with that of selected S reference standards, including pyrite, elemental S, mackinawite, greigite and aqueous SO_4^{2-}. The S standards were prepared as described in Burton et al. (2009).

Statistical analysis

Bivariate correlations were undertaken to determine the linear association between two quantitative variables. Frequency histograms and distribution statistics were used to determine departures from normality. Due to non-normal distribution, Spearman's rho correlation coefficients were used to examine the significance level of the linear relationship. All statistical analyses were conducted with SPSS Statistics 17.0.

Results and discussion

General sediment characteristics

At the Firewood Creek site, the former ASS subjected to reintroduction of tidal inundation (M and MF) were classified as Typic Sulfaquents according to Soil Taxonomy (Soil Survey Staff 2006). Sediment pH was circumneutral with a pH_F range from 6.24 to 7.38, and measured Eh_F values were indicative of moderately reducing conditions, with a redox potential from −65 to +159 mV at M and MF (Table 2). Values are consistent with those reported by Johnston et al. (2009b). Surface mangrove sediments at the reference site (TI) were generally more oxidised, with a mean pH_F of 6.3 and redox potential of +163 mV (Table 2). This may be explained by factors such as bioturbation, the presence of roots, or tidal flushing, which are known to promote oxic conditions in intertidal mangrove environments (e.g., Nickerson and Thibodeau 1985; Holmer et al. 1994). The organic-rich mangrove sediments in this vicinity were generally classified as Typic Sulfihemists or Typic Sulfisaprists (Soil Survey Staff 2006) by Hicks et al. (1999).

Molar ratios of water-soluble $Cl:SO_4$ reflected the modern supply of marine salts in the 3 physiographic settings (Table 2). In TI mangrove sediments, high seawater supply and tidal flushing promoted greater sulfate reduction than in the tidally inundated ASS (M and MF), indicated by excess Cl^- and higher $Cl:SO_4$ ratios. A ratio of ~20 is characteristic of seawater (e.g., Holmer et al. 1994; Portnoy and Giblin 1997).

The profile distributions of total C, Fe and S concentrations (mean ± 1 SD of three profiles) in tidally inundated ASS are shown in Fig. 2. Large amounts of total C were evident in surface soils (0–0.05 m depth) at M (4807 ± 546 μmol/g), which decreased to a minimum of 1268 ± 89 μmol/g in the former sulfuric horizon. Similarly, M contained greater total Fe (3257 ± 640 μmol/g) and S (241 ± 24 μmol/g) in the surface soils than those at MF (Fig. 2).

In the TI mangrove sediments, total C and S contents were either equivalent (0–0.05 m depth) or considerably larger (0.05–0.15 m depth) than those for tidally inundated ASS. However, total Fe contents were substantially smaller in TI surface sediments (with a difference of 2889 μmol/g), and similar to the total Fe pool in M and MF soils at depth (Fig. 2). These values are typical of estuarine sediments in an intertidal mangrove wetland (Burton et al. 2006a; Otero et al. 2009).

Solid phase Fe fractionation

Solid phase reactive Fe fractions of soil profiles (mean ± 1 SD of three profiles analysed in triplicate) for tidally inundated ASS are shown in Fig. 3. Of these fractions, HCl-extractable Fe(II) was most abundant in the surface sediments (0–0.05 m depth), with concentrations of 1243 ± 289 μmol/g at M and 742 ± 402 μmol/g at MF. These values were considerably greater than HCl-extractable Fe(III) at the same depth interval, with maximum concentrations of 583 ± 124 μmol/g at M and 513 ± 414 μmol/g at MF. Maximum dithionite-extractable Fe concentrations of 908 ± 383 μmol/g at M and 468 ±

Table 2 Selected properties of surface soils and sediments (0–0.05 m depth) from the three physiographic settings examined in this study

Site	pH_F		Eh_F (mV; SHE)		θ_g (g/g)		$\sum$ soluble cations ($mmol_c/kg$)		Soluble Cl^- ($mmol_c/kg$)		Molar Cl^-/SO_4^{2-}
	$\overline{x}$	s	$\overline{x}$	s	$\overline{x}$	s	$\overline{x}$	s	$\overline{x}$	s	$\overline{x}$
M	7.05	0.08	−16	41	1.47	0.23	391	151	311	111	9
MF	7.17	0.18	18	86	0.93	0.17	386	98	306	64	13
TI	6.35	0.24	171	23	1.66	0.12	806	67	748	66	8

Data represent the mean ± 1 SD of three profiles

M vegetated ASS mudflat, *MF* unvegetated ASS mudflat, *TI* Trinity Inlet mangrove wetland

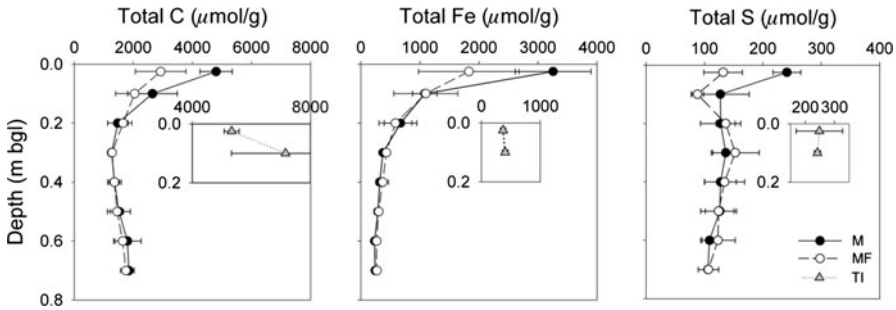

Fig. 2 Profile distributions of selected geochemical characteristics in soils and sediments from M, MF and TI sampling sites. Data points represent the mean ± 1 SD of three profiles

178 μmol/g at MF also occurred in the surface sediments (0–0.05 m depth). For all tidally inundated ASS profile distributions, there was a sharp decrease in reactive Fe fractions with depth (Fig. 3).

From a broader perspective, concentrations of HCl-extractable total Fe (which includes Fe(II) and Fe(III) fractions) in tidally inundated ASS at M and MF (0–0.05 m depth) were almost an order of magnitude greater than those surface sediments (0–0.04 m depth) reported for other coastal marine and intertidal estuarine environments (Fig. 4). In contrast, background levels of HCl-extractable total Fe in the undrained, mangrove sediments at TI were comparable to values reported in previous studies of

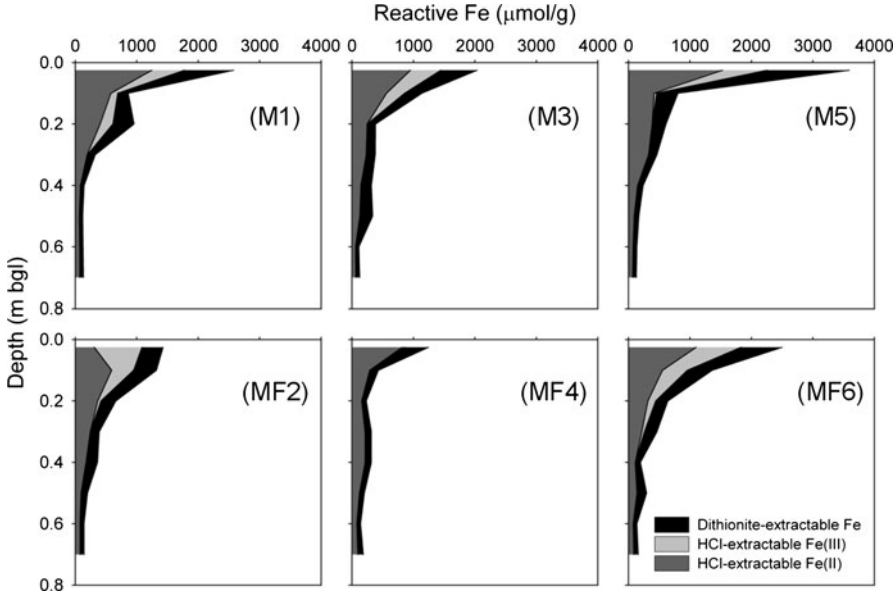

Fig. 3 Abundance of reactive Fe fractions (μmol/g) in tidally inundated ASS profiles from vegetated (M) and unvegetated (MF) mudflat sampling sites. Data points represent the mean of triplicate analyses

mangrove and saltmarsh sediments (Fig. 4, Holmer et al. 1994; Otero and Macías 2002). Moreover, dithionite-extractable Fe concentrations in surface sediments were greater at M and MF than those at TI (123 ± 30 μmol/g, Table 3).

Total Fe content in tidally inundated ASS spanned a wide range of 224–3967 μmol/g (Fig. 2; Table 3). Importantly, reactive Fe (HCl- plus dithionite-extractable fractions minus AVS–Fe) comprised almost 90% of the total Fe at M and MF in the upper 0.35 m, and decreased to 50–80% of total Fe below this depth (Table 3). These smaller reactive Fe contents at depth were similar to those concentrations found in the TI mangrove sediments (Table 3), indicating that the enrichment of reactive Fe is largely confined to surface sediments. This is consistent with observations at the Firewood Creek site where surficial accumulations of Fe(III) minerals were poorly crystalline and comprised mainly of schwertmannite with minor quantities of goethite and lepidocrocite, directly observed by X-ray powder diffractometry (XRPD) and scanning electron microscopy (SEM) (Johnston et al. 2010a).

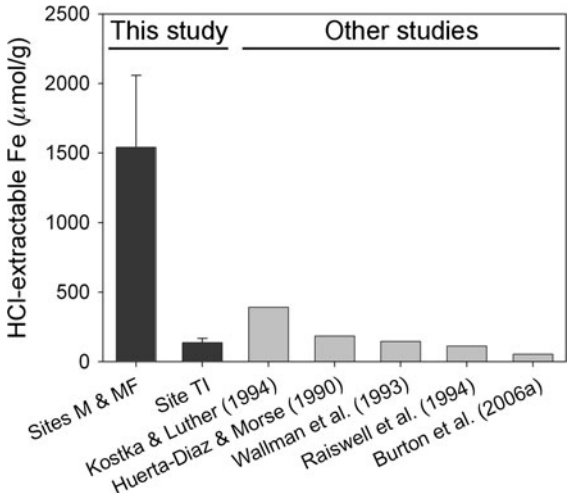

Fig. 4 Comparison of HCl-extractable total Fe concentrations in surface soils and sediments (0–0.05 m depth) from M, MF and TI sampling sites with previously reported data for coastal marine and estuarine sediments. Data points from this study represent the mean ± 1 SD of triplicate analyses. Results from other studies are based on surface sediments (0–0.04 m depth) with a 0.5–1 M HCl extraction time of 1–24 h

AVS–Fe represented only a small proportion (generally <5%) of total Fe in tidally inundated ASS (up to 57 μmol/g at M; 38 μmol/g at MF, Table 3). Pyrite–Fe was also present at relatively small concentrations (7–30 μmol/g at M; 9–28 μmol/g at MF, Table 3) and consequently comprised a small proportion of total Fe. Amounts of these iron sulfide mineral phases were overshadowed by concentrations of reactive Fe fractions, which dominated at all depths. With increasing depth, AVS–Fe accounted for a smaller portion of the total Fe pool and pyrite–Fe accounted for a concomitantly larger portion in the tidally inundated ASS. The accumulation of AVS can be limited due to its transformation to pyrite, which generally represents an important sink for reactive Fe species in sulfidic materials (e.g., Burton et al. 2006a, b). The residual Fe fraction is likely to be associated with Fe bound within the lattice structure of crystalline silicate minerals; this Fe is relatively unreactive with porewater sulfides (Canfield et al. 1992; Kostka and Luther 1995).

This result for tidally inundated ASS contrasted with the TI mangrove sediments, where a larger proportion of the total Fe pool was pyrite–Fe (~20%) and a much smaller fraction was AVS–Fe (<1%, Table 3). Concentrations of pyrite–Fe in the TI mangrove sediments were greater than that determined at all depth intervals in the tidally inundated ASS. In addition, poorly crystalline Fe accounted for only 25–37% of total Fe in the TI mangrove sediments, which was considerably smaller than the proportion measured in the surface soils at M and MF.

The reactivity of iron minerals towards sulfide is of major importance for the formation of RIS species. The surface soils at M and MF contained extraordinarily large concentrations of reactive Fe. The DOP estimates the amount of Fe available for reaction with sulfide over geologic time (Berner 1970), and is defined as:

$$\mathrm{DOP} = \mathrm{Pyrite{-}Fe}/(\mathrm{Pyrite{-}Fe} + \mathrm{Reactive\ Fe}) \quad (4)$$

However, in sediments that contain a significant solid phase fraction of AVS, the DOP approach does not provide a good estimate the availability of reactive Fe over the much shorter time scales during early diagenesis. In these sediments, the effect of reactive Fe availability on sulfide accumulation may

Table 3 Speciation of solid phase Fe and degree of sulfidisation in soil and sediment profiles from M, MF and TI sampling sites

Depth (m)	AVS–Fe (μmol/g)		Poorly crystalline Fe (μmol/g)		Crystalline Fe (μmol/g)		Pyrite–Fe (μmol/g)		Total Fe (μmol/g)		DOS (%)
	$\bar{x}$	s	$\bar{x}$	s	$\bar{x}$	s	$\bar{x}$	s	$\bar{x}$	s	$\bar{x}$
Site M											
0–0.05	57	5	1769	410	908	383	10	2	3257	640	2.6
0.05–0.15	30	16	639	193	265	90	7	3	1083	207	4.0
0.65–0.75	0	0	69	5	58	2	30	4	241	25	17.9
Site MF											
0–0.05	46	39	1218	508	468	177	9	10	1832	852	3.5
0.05–0.15	9	5	728	379	298	152	10	14	1101	543	3.5
0.65–0.75	0	0	87	9	73	12	28	3	272	19	15.0
Site TI											
0–0.05	1	0	137	28	123	29	67	18	368	46	21.4
0.05–0.15	3	4	99	28	103	24	85	20	405	49	28.7

Data represent the mean ± 1 SD of three profiles

then be described by the degree of sulfidisation (DOS) (Boesen and Postma 1988):

$$\mathrm{DOS} = (\mathrm{Pyrite{-}Fe} + \mathrm{AVS{-}Fe})/(\mathrm{Pyrite{-}Fe} + \mathrm{AVS{-}Fe} + \mathrm{Reactive\ Fe}) \quad (5)$$

where reactive Fe is the HCl- plus dithionite-extractable Fe minus AVS–Fe.

In the tidally inundated ASS, DOS values were small (~3%, Table 3), indicating that sulfidisation was not limited by the availability of reactive Fe in surface materials. Relatively higher DOS and lower DOP values also suggested that the conversion of AVS to pyrite may be inhibited in the surface soils at M and MF. In contrast, DOP and DOS exceeded 21% in TI mangrove sediments. These values were closer to DOS at depth in M and MF soils (Table 3). Burton et al. (2006a) found DOS was up to 100% in near surface mangrove sediments. The extraction technique used to define reactive Fe (Leventhal and Taylor 1990) and the assumed AVS stoichiometry of FeS (Rickard and Morse 2005) were considered to have minimal effect on DOS determinations in these tidally inundated ASS and mangrove sediments.

Solid phase S fractionation

Solid phase RIS fractions of soil profiles for tidally inundated ASS are shown in Fig. 5. Maximum AVS–S concentrations of 57 ± 5 μmol/g at M and 46 ± 39 μmol/g at MF occurred in the surface soils (0–0.05 m depth). These values are comparable with AVS found in other marine and estuarine sediments (<90 μmol/g, Morse and Cornwell 1987; Burton et al. 2005) where AVS accumulation is generally limited by progressive transformation to pyrite. However, abundant preservation of metastable iron sulfides in anoxic, brackish-water ASS sediments has been recently reported for the boreal zone (up to 0.88%, Boman et al. 2010). AVS–S concentrations decreased with depth in all tidally inundated ASS profiles. In contrast, maximum AVS–S (2.6 ± 2.6 μmol/g) in the TI mangrove sediments was at least an order of magnitude less than values in M and MF soils.

To identify the AVS mineral component of sedimentary sulfides in the tidally inundated ASS, XANES absorption spectra of selected soils were compared to a series of S reference standards and are shown in Fig. 6. All samples displayed white line peak energies of ~2481 eV consistent with SO_4^{2-}, which could be free sulfate in solution or sulfate contained in a mineral phase. With abundant AVS–S, M and MF surface soils (0–0.05 m depth) displayed peak energy positions closest to that of greigite. Minor differences occur in peak shape, which suggest chemical differences between the soils and the standards. The MF soil sample taken at 0.35–0.45 m depth is consistent with the peak energy position for either elemental S and/or pyrite. Pyrite and elemental S have rising edges that are very close

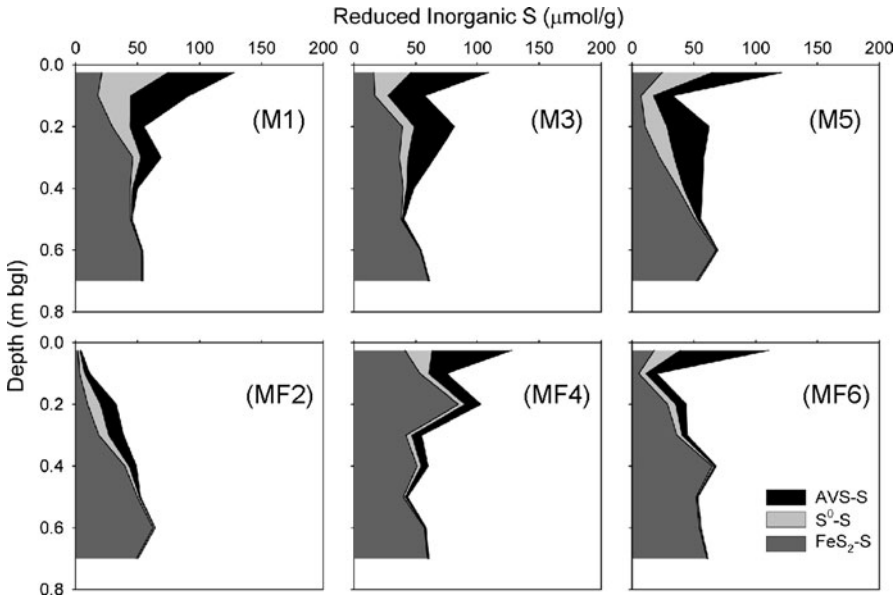

Fig. 5 Abundance of RIS fractions (μmol/g) in tidally inundated ASS profiles from vegetated (M) and unvegetated (MF) mudflat sampling sites. Data points represent the mean of triplicate analyses

in energy (~2471.1 eV) which makes it difficult to differentiate between the two based on S K-edge data alone (Morgan et al. 2009). Extraction data indicate that pyrite was the dominant RIS fraction in this sample (Fig. 5). In natural systems, differences in peak intensities can be related to particle size and concentration effects (Morgan et al. 2009). From the XANES data shown, it is clear that the RIS chemistry of the tidally inundated ASS was dominated by Fe–S mineral phases. This is consistent with AVS accumulation in the surface soils and increased pyrite at depth. Direct evidence of metastable AVS mineral phases such as greigite has rarely been presented for intertidal estuarine systems (e.g., Rickard and Morse 2005).

In the tidally inundated ASS, S^0–S was generally most abundant in the surface soils (0–0.05 m depth), with concentrations of 41 ± 12 μmol/g at M and 15 ± 11 μmol/g at MF (Fig. 5). S^0–S decreased with depth in a similar manner to that of AVS–S. These S^0–S concentrations are comparable to those present in some estuarine and marine sediments (< 50 μmol/g, Thode-Andersen and Jørgensen 1989; Burton et al. 2006a), but less than those reported for some ASS drain sediments (up to 396 μmol/g, Burton et al. 2006b). In TI mangrove sediments, S^0–S concentrations were very small (3.6 ± 0.9 μmol/g). The formation of S^0 via SO_4^{2-} reduction (Thode-Andersen and Jørgensen 1989) is an important pathway leading

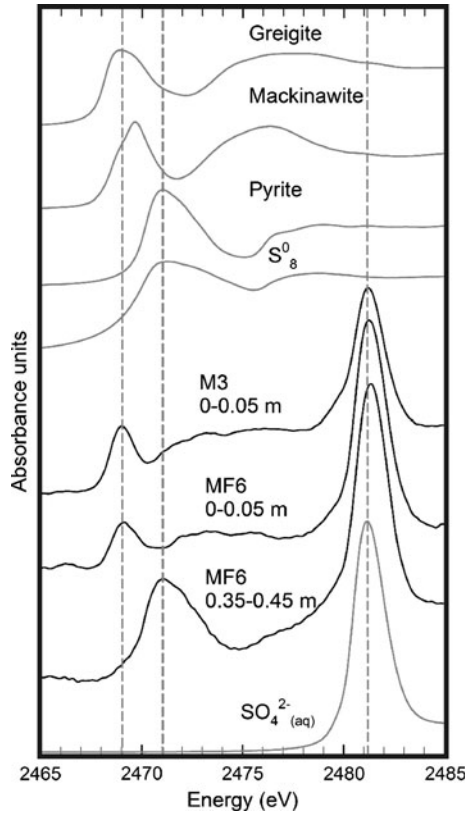

Fig. 6 Sulfur K-edge XANES spectra of selected surface (0–0.05 m depth) and subsurface (0.35–0.45 m depth) soils from M and MF sampling sites in comparison to S standards. *Vertical dashed lines* denote the prominent white-line positions of the XANES spectra for the samples

to the formation of pyrite and involving FeS clusters (Berner 1970; Rickard 1974).

Total S content in the tidally inundated ASS spanned a range of 88–241 μmol/g (Fig. 2). A large proportion of this total S (generally >40%) was composed of RIS (Fig. 7a). Pyrite–S contents in M and MF soils generally increased with depth from a minimum of 14 ± 6 μmol/g (0.05–0.15 m depth) to a maximum of 58 ± 8 μmol/g (0.65–0.75 m depth, Fig. 5), where pyrite–S comprised the largest fraction of the total S pool (up to 54%, Fig. 7a). In TI mangrove sediments, pyrite–S was between 135 ± 37 and 157 ± 55 μmol/g and up to 66% of total S (Fig. 7a). This was more than twice the pyrite–S concentrations determined in the tidally inundated ASS, yet is comparable to those levels typically present in marine and estuarine sediments (Holmer et al. 1994; Burton et al. 2006a; Otero et al. 2009).

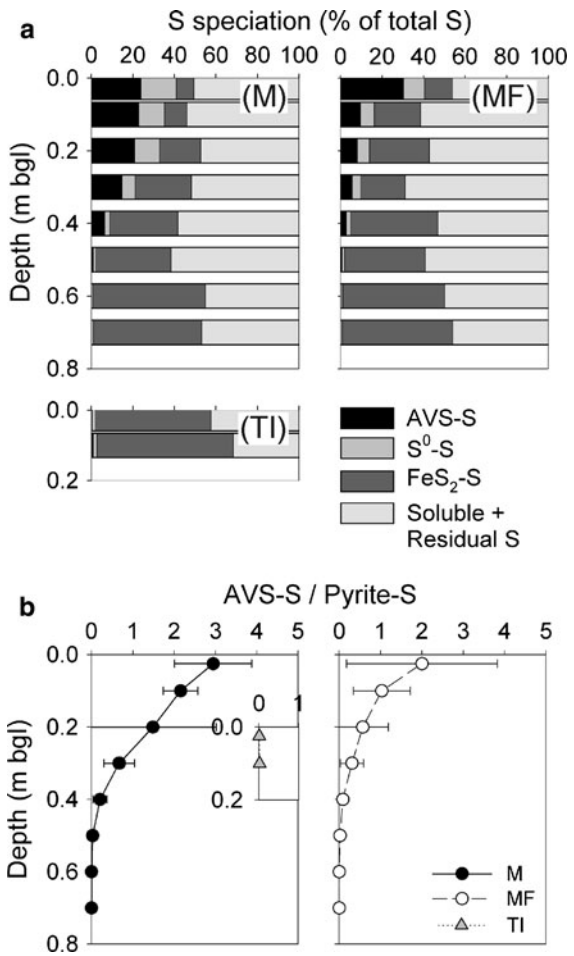

Fig. 7 Speciation of solid phase S (**a**) and AVS–S to pyrite–S ratios (**b**) in soil and sediment profiles from M, MF and TI sampling sites. Data points represent the mean of triplicate profiles, with ± 1 SD for **b**

In most estuarine sedimentary systems, pyrite generally dominates the RIS fractions, with AVS and S^0 typically comprising only a minor fraction of total RIS (Giblin and Wieder 1992; Morse and Rickard 2004). However, AVS–S and S^0–S were the dominant forms of RIS in M and MF surface soils (generally >70%, Fig. 5), and comprised ~40% of the total S (Fig. 7a). In contrast, AVS–S and S^0–S comprised only a very small proportion of the RIS formed in TI mangrove sediments. Over geological time, these sedimentary sulfides may be progressively transformed to the more stable pyrite, resulting in decreasing AVS–S to pyrite–S ratios (Morse and Rickard 2004). AVS–S to pyrite–S ratios decreased with depth in M and MF soil profiles and are shown in Fig. 7b. The tidally inundated ASS were characterised by high AVS–S to pyrite–S ratios in the surface soils at M (up to 2.94) and MF (up to 2.00), indicating a low degree of conversion of AVS minerals to pyrite. These ratios are similar to the high values found in ASS drain sediments by Burton et al. (2006b) and in coastal marine sediments by Middelburg (1991) and Gagnon et al. (1995) that were considered anomalous, given conditions were conducive to pyrite formation. In contrast, TI mangrove sediments contained very low AVS–S to pyrite–S ratios (Fig. 7b), indicating an efficient conversion of AVS to pyrite. A number of biogeochemical parameters may explain the favoured AVS accumulation relative to that of pyrite, such as sediment deposition rates, redox conditions and iron availability (Thode-Andersen and Jørgensen 1989; Middelburg 1991; Gagnon et al. 1995). In fact, preservation of metastable iron sulfide is primarily controlled by limited sulfur supply, an abundance of Fe(II) and strongly reducing conditions in boreal brackish-water sediments (Boman et al. 2010). In these estuarine tidally inundated ASS, it is most likely that the persistence of AVS occurs as a result of the abundant reactive Fe favouring S sequestration in FeS (Canfield 1989; Gagnon et al. 1995; Boman et al. 2010).

Fe and S cycling—hysteresis of tidal remediation

Our results suggest that very large concentrations of reactive Fe in the tidally inundated ASS have exerted

a substantial influence on sulfidisation processes and RIS speciation in the near surface materials. Strong positive relationships were observed between poorly crystalline Fe and AVS–S ($r = 0.83$; $n = 54$) and S^0–S ($r = 0.85$; $n = 54$) concentrations, significant at the 0.01 level, and are shown in Fig. 8. This is consistent with abundant reactive Fe favouring the accumulation of AVS minerals and S^0 relative to that of pyrite in these soils (Burton et al. 2006b). It also suggests that the accumulation of pyrite in the tidally inundated ASS may be occurring slowly under the described geochemical conditions. The kinetics of RIS formation and speciation may reflect the relatively short time scale of remediation via tidal inundation ($\sim$5 years) at this site.

The reintroduction of tidal inundation to ASS has initiated similar diagenetic forces to those occurring in the undrained, intertidal mangrove sedimentary environment (i.e., reducing conditions, regular tidal inundation, abundant organic C, supply of marine derived SO_4^{2-}). However, the contemporary situation differs significantly from the historical environment, as there is now a far greater pool of reactive Fe in surface soils. This increase in the availability of reactive Fe has profound consequences for the coupled cycling of Fe and S, and is likely to cause a distinct hysteresis during the reformation of pyrite. This hysteresis can be represented by a conceptual model of biogeochemical cycling of reactive Fe and pyrite–S (Fig. 9a).

In this model, initial pyrite-rich, estuarine sediments (*1*) are oxidised due to the exclusion of tides and drainage of sediment. This oxidative process leads to (*2*), where pyrite–S is exhausted, thereby liberating acidity, Fe and SO_4^{2-}, and forming secondary Fe(III) minerals (Hicks et al. 1999; Johnston et al. 2010a, b). Following the reintroduction of tidal inundation, reductive dissolution of these Fe(III) minerals generates abundant Fe(II) in porewaters. Subsequent oxidation of porewater Fe(II) in interfacial sediments leads to the surface enrichment of reactive Fe (Johnston et al. 2010b) and is contemporaneous with SO_4^{2-} reduction (*3*). Over time, the pool of reactive Fe is likely to be transformed via continued sulfidisation (*1*), leading to increasing pyrite accumulation in these soils.

This conceptual model is supported by measured field data from surface estuarine sediments (Fig. 9b). Undrained TI mangrove sediments (*1*) generally exhibited large pyrite–S contents and a small reactive Fe fraction (Fig. 9b), typical of sulfide-rich material deposited during the Holocene. In drained and oxidised surface ASS (*2*), the store of pyrite was consumed and the proportion of reactive Fe had increased. After reintroduction of tidal inundation (*3*), further enrichment of poorly crystalline Fe occurred and pyrite–S began to form in the surface M and MF soils.

Implications of enriched reactive Fe for sulfidisation—short and long-term consequences

In tidally inundated ASS landscapes, a major short-term consequence of enriched reactive Fe is the preferential formation and accumulation of reactive RIS species (such as AVS and S^0) in surface soils. In such situations, accumulation of these RIS fractions during tidal remediation poses a significant hazard (cf. accumulation as pyrite), as the oxidation of AVS and S^0 occurs far more rapidly than the oxidation of

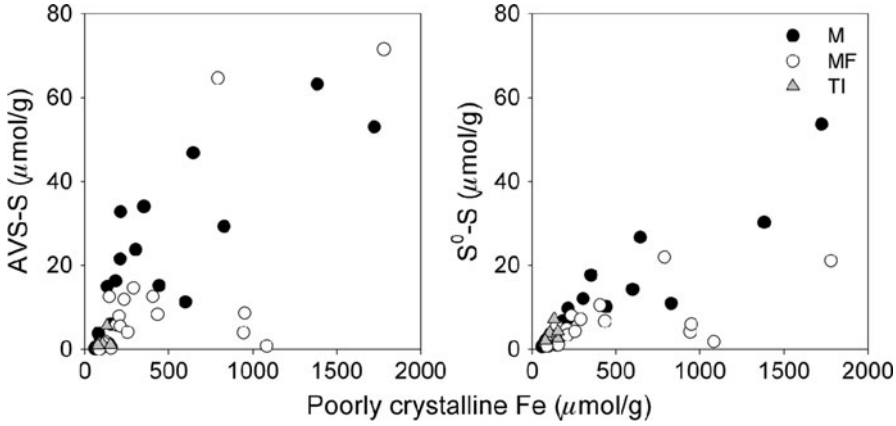

Fig. 8 Bivariate relationships of solid phase AVS–S ($r = 0.83$) and S^0–S ($r = 0.85$) with poorly crystalline Fe in soils and sediments from M, MF and TI sampling sites ($n = 54$). Data points represent the mean of triplicate analyses

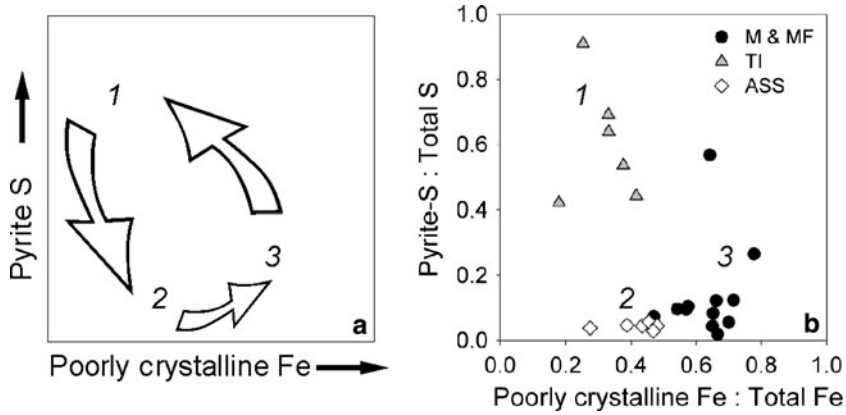

Fig. 9 Conceptual representation of hysteresis in poorly crystalline Fe and pyrite–S fractions of a tidally inundated surface ASS (**a**), where *1* refers to undrained, pyrite-rich, intertidal mangrove sediments; *2* refers to drainage of sediments due to tidal exclusion, causing pyrite oxidation and secondary Fe(III) mineral formation; and *3* refers to restoration of tidal inundation to soils, reductive dissolution of Fe(III) minerals, surface diagenetic enrichment of poorly crystalline Fe and reformation of pyrite–S. Field data for surface materials (mean of 0–0.15 m depth) at the Firewood Creek site (**b**) under natural (*1*; TI) and drained (*2*; from Johnston et al. 2009b) conditions, and after the reintroduction of tidal inundation (*3*; M and MF)

pyrite (e.g., Bush and Sullivan 1997; Burton et al. 2009). Closure of the tidal floodgates and cessation of tidal inundation may lead to rapid oxidation, acidification and reversal of remediation at the East Trinity field site.

However, further transformation of AVS and S^0 to the more stable pyrite is likely over the long term, given continued tidal inundation. Reactive Fe is one of the primary factors controlling the formation of pyrite in intertidal sedimentary environments (e.g., Canfield 1989; Canfield et al. 1992). Hence, its surface enrichment may eventually promote elevated pyrite contents with sufficient time. TI mangrove sediments provide a local DOS reference value that can be used to estimate the likely future extent of sulfidisation in surface soils. The mean DOS value for TI mangrove sediments was 22% (Table 3) and reactive Fe content for the tidally inundated ASS (M and MF) ranged from 1179 to 3534 µmol/g at the same depth interval (0–0.05 m). By substituting in Eq. 4, we can use these DOS values to infer a theoretical value for pyrite–Fe in the tidally inundated ASS which accounts for the enriched reactive Fe. Assuming conservative mass behaviour and no change in AVS–S content, this equates to a pyrite–Fe content ranging from 189 to 704 µmol/g. This is equivalent to a pyrite content of 2–8% g/g in surface soils, which is higher than values determined prior to drainage by an order of magnitude (0.8% pyrite g/g in TI mangrove sediments). DOP and DOS values of 80–100% are typical of intertidal mangrove sedimentary environments (Burton et al. 2006a; Otero et al. 2009). If such DOS were achieved in these tidally inundated ASS materials, this could eventually result in pyrite up to 42% g/g at the soil surface.

The kinetics of further sulfidisation in Fe-enriched ASS landscapes are yet to be quantified. However, the potential for elevated pyrite contents in surface soils has implications for ongoing site management and may prove to be an important feature of tidal remediation in ASS wetlands. This is particularly relevant given predicted sea-level rise associated with a warming global climate (Solomon et al. 2007). The enhanced accumulation of AVS minerals and pyrite in coastal ASS landscapes over the longer term, whether a result of planned remediation by the re-establishment of tidal inundation or by rising sea levels consequent of climate change, has important implications for many estuarine sedimentary environments around the world.

Conclusions

This study examined solid phase Fe and S partitioning following tidal inundation of a previously drained ASS wetland. An exceptional diagenetic enrichment of reactive Fe(III) oxides occurred in surface soils.

Reactive Fe accounted for almost 90% of the total Fe pool in tidally inundated ASS and exerted a major control on the formation, speciation and transformation of RIS. AVS and elemental sulfur (S^0) comprised dominant fractions of RIS species in these surface soils. Large AVS–S to pyrite–S ratios in soils containing abundant reactive Fe indicated an inefficient conversion of AVS minerals to pyrite. Large availability of reactive Fe favoured formation and accumulation of AVS minerals and S^0 relative to pyrite, despite geochemical conditions being conducive to pyrite formation. This appears to be related to the short time period ($\sim$5 years) of tidal inundation of ASS and is associated with early diagenesis. Reactive RIS fractions in surface soils are likely to oxidise rapidly and cause acidification were tidal inundation ceased. However, the enrichment of reactive Fe may promote the enhanced sequestration of S within pyrite over the longer term. The geochemical cycling of reactive Fe and RIS in tidally inundated ASS is toward increased sulfidisation, yet this pathway displays a distinct hysteresis. These findings provide an important new understanding of sulfidisation in tidally inundated ASS landscapes enriched in reactive Fe.

Acknowledgements We would like to thank the Queensland Department of Environment and Resource Management (DERM) who facilitated this research and the assistance of DERM staff at the East Trinity field site is gratefully acknowledged. Synchrotron access was funded by the Australian Synchrotron Research Program and the National Synchrotron Radiation Research Centre (NSRRC) in Taiwan, and we thank Dr Rosalie Hocking of Monash University, Australia and Dr L-Y Jang of NSRRC, Taiwan for their assistance with XANES data collection. This research was supported by the Cooperative Research Centre for Contamination Assessment and Remediation of the Environment (Project No. 6-6-01-06/07). We thank the Editor and reviewers for their constructive comments on this manuscript.

References

APHA-AWWA-WEF (2005) Standard methods for the examination of water and wastewater. American Public Health Association, American Water Works Association and Water Environment Federation, Baltimore

Bartlett JK, Skoog DA (1954) Colorimetric determination of elemental sulfur in hydrocarbons. Anal Chem 26:1008–1011

Berner RA (1970) Sedimentary pyrite formation. Am J Sci 268:1–23

Boesen C, Postma D (1988) Pyrite formation in anoxic environments of the Baltic. Am J Sci 288:575–603

Boman A, Åström M, Fröjdö S (2008) Sulfur dynamics in boreal acid sulfate soils rich in metastable iron sulfide—the role of artificial drainage. Chem Geol 255:68–77

Boman A, Fröjdö S, Backlund K, Åström ME (2010) Impact of isostatic land uplift and artificial drainage on oxidation of brackish-water sediments rich in metastable iron sulfide. Geochim Cosmochim Acta 74:1268–1281

Bureau of Meteorology (2010) Monthly climate statistics for Cairns Aero. Commonwealth of Australia, Canberra. http://www.bom.gov.au/climate/averages. Accessed 29 Mar 2010

Burton ED, Phillips IR, Hawker DW (2005) Reactive sulfide relationships with trace metal extractability in sediments from southern Moreton Bay, Australia. Mar Pollut Bull 50:589–595

Burton ED, Bush RT, Sullivan LA (2006a) Fractionation and extractability of sulfur, iron and trace elements in sulfidic sediments. Chemosphere 64:1421–1428

Burton ED, Bush RT, Sullivan LA (2006b) Reduced inorganic sulfur speciation in drain sediments from acid sulfate soil landscapes. Environ Sci Technol 40:888–893

Burton ED, Bush RT, Sullivan LA, Mitchell DRG (2007) Reductive transformation of iron and sulfur in schwertmannite-rich accumulations associated with acidified coastal lowlands. Geochim Cosmochim Acta 71:4456–4473

Burton ED, Bush RT, Sullivan LA, Mitchell DRG (2008a) Schwertmannite transformation to goethite via the Fe(II) pathway: reaction rates and implications for iron-sulfide formation. Geochim Cosmochim Acta 72:4551–4564

Burton ED, Sullivan LA, Bush RT, Johnston SG, Keene AF (2008b) A simple and inexpensive chromium-reducible sulfur method for acid-sulfate soils. Appl Geochem 23:2759–2766

Burton ED, Bush RT, Sullivan LA, Hocking RK, Mitchell DRG, Johnston SG, Fitzpatrick RW, Raven M, McClure S, Jang LY (2009) Iron-monosulfide oxidation in natural sediments: resolving microbially mediated S transformations using XANES, electron microscopy, and selective extractions. Environ Sci Technol 43:3128–3134

Bush RT, Sullivan LA (1997) Morphology and behaviour of greigite from a Holocene sediment in eastern Australia. Aust J Soil Res 35:853–861

Bush RT, Fyfe D, Sullivan LA (2004) Occurrence and abundance of monosulfidic black ooze in coastal acid sulfate soil landscapes. Aust J Soil Res 42:609–616

Canfield DE (1989) Reactive iron in marine sediments. Geochim Cosmochim Acta 53:619–632

Canfield DE, Raiswell R, Westrich JT, Reaves CM, Berner RA (1986) The use of chromium reduction in the analysis of reduced inorganic sulfur in sediments and shales. Chem Geol 54:149–155

Canfield DE, Raiswell R, Bottrell S (1992) The reactivity of sedimentary iron minerals towards sulfide. Am J Sci 292:659–683

Cornwell JC, Morse JW (1987) The characterization of iron sulfide minerals in anoxic marine sediments. Mar Chem 22:193–206

Dent D (1986) Acid sulphate soils: a baseline for research and development. ILRI Publication 39. International Institute for Land Reclamation & Improvement, Wageningen

Fältmarsch RM, Åström ME, Vuori K-M (2008) Environmental risks of metals mobilised from acid sulphate soils in Finland: a literature review. Boreal Environ Res 13:444–456

Gagnon C, Mucci A, Pelletier E (1995) Anomalous accumulation of acid-volatile sulphides (AVS) in a coastal marine sediment, Saguenay Fjord, Canada. Geochim Cosmochim Acta 59:2663–2675

Giblin AE, Howarth RW (1984) Porewater evidence for a dynamic sedimentary iron cycle in salt marshes. Limnol Oceanogr 29:47–63

Giblin AE, Wieder RK (1992) Sulfur cycling in marine and fresh wetlands. In: Howarth RW, Stewart JWB, Ivanov MV (eds) Sulfur cycling on the continents: wetlands, terrestrial ecosystems and associated water bodies. Wiley, Chichester, pp 85–117

Hicks WS, Bowman GM, Fitzpatrick RW (1999) East Trinity acid sulfate soils. Part 1: Environmental hazards. Technical Report 14/99. CSIRO Land & Water, Adelaide, p 79

Hicks W, Fitzpatrick RW, Bowman G (2003) Managing coastal acid sulfate soils: the East Trinity example. In: Roach IC (ed) Advances in regolith: Proceedings of the CRC LEME regional regolith symposia. CRC LEME, Bentley, pp 174–177

Holmer M, Kristensen E, Banta G, Hansen K, Jensen M, Bussawarit N (1994) Biogeochemical cycling of sulfur and iron in sediments of a south-east Asian mangrove, Phuket Island, Thailand. Biogeochemistry 26:145–161

Howarth RW, Jørgensen BB (1984) Formation of ^{35}S-labelled elemental sulfur and pyrite in coastal marine sediments (Limfjorden and Kysing Ford, Denmark) during short-term $^{35}SO_4^{2-}$ reduction measurements. Geochim Cosmochim Acta 48:1807–1818

Hsieh YP, Chung SW, Tsau YJ, Sue CT (2002) Analysis of sulfides in the presence of ferric minerals by diffusion methods. Chem Geol 182:195–201

Huerta-Díaz MA, Morse JW (1990) A quantitative method for determination of trace metal concentrations in sedimentary pyrite. Mar Chem 29:119–144

Johnston SG, Bush RT, Sullivan LA, Burton ED, Smith D, Martens MA, McElnea AE, Ahern CR, Powell B, Stephens LP, Wilbraham ST, van Heel S (2009a) Changes in water quality following tidal inundation of coastal lowland acid sulfate soil landscapes. Estuar Coast Shelf Sci 81:257–266

Johnston SG, Keene AF, Bush RT, Burton ED, Sullivan LA, Smith D, McElnea AE, Martens MA, Wilbraham S (2009b) Contemporary pedogenesis of severely degraded tropical acid sulfate soils after introduction of regular tidal inundation. Geoderma 149:335–346

Johnston SG, Burton ED, Bush RT, Keene AF, Sullivan LA, Smith D, McElnea AE, Ahern CR, Powell B (2010a) Abundance and fractionation of Al, Fe and trace metals following tidal inundation of a tropical acid sulfate soil. Appl Geochem 25:323–335

Johnston SG, Keene AF, Burton ED, Bush RT, Sullivan LA, McElnea AE, Ahern CR, Smith CD, Powell B, Hocking RK (2010b) Arsenic mobilization in a seawater inundated acid sulfate soil. Environ Sci Technol 44:1968–1973

Kostka JE, Luther GW (1994) Partitioning and speciation of solid phase iron in saltmarsh sediments. Geochim Cosmochim Acta 7:1701–1710

Kostka JE, Luther GW (1995) Seasonal cycling of Fe in saltmarsh sediments. Biogeochemistry 29:159–181

Lax K (2005) Stream plant chemistry as indicator of acid sulphate soils in Sweden. Agric Food Sci 14:83–97

Leventhal J, Taylor C (1990) Comparison of methods to determine degree of pyritization. Geochim Cosmochim Acta 54:2621–2625

Lord CJ, Church TM (1983) The geochemistry of salt marshes: sedimentary ion diffusion, sulfate reduction, and pyritization. Geochim Cosmochim Acta 47:1381–1391

Lovely DR, Phillips EJP (1987) Competitive mechanisms for inhibition of sulfate reduction and methane production in the zone of ferric iron reduction in sediments. Appl Environ Microbiol 53:2636–2641

Luther GW, Ferdelman TG, Kostka JE, Tsamabis EJ, Church TM (1991) Temporal and spatial variability of reduced sulfur species (FeS_2, $S_2O_3^{2-}$) and porewater parameters in salt marsh sediments. Biogeochemistry 14:57–88

Macdonald BCT, Smith J, Keene AF, Tunks M, Kinsela A, White I (2004) Impacts of runoff from sulfuric soils on sediment chemistry in an estuarine lake. Sci Total Environ 329:115–130

Middelburg JJ (1991) Organic carbon, sulphur, and iron in recent semi-euxinic sediments of Kau Bay, Indonesia. Geochim Cosmochim Acta 55:815–828

Morgan KE, Burton ED, Cook P, Raven MD, Fitzpatrick RW, Bush RT, Sullivan LA, Hocking RK (2009) Fe and S K-edge XAS determination of iron-sulfur species present in a range of acid sulfate soils: effects of particle size and concentration on quantitative XANES determinations. 14th international conference on x-ray absorption fine structure (XAFS14). J Phys Conf Ser 190:012144

Morse JW, Cornwell JC (1987) Analysis and distribution of iron sulfide minerals in recent anoxic marine sediments. Mar Chem 22:55–69

Morse JW, Rickard D (2004) Chemical dynamics of sedimentary acid volatile sulfide. Environ Sci Technol 38:131A–136A

Nickerson NH, Thibodeau FR (1985) Association between pore water sulfide concentrations and the distribution of mangroves. Biogeochemistry 1:183–192

Otero XL, Macías F (2002) Variation with depth and season in metal sulfides in salt marsh soils. Biogeochemistry 61:247–268

Otero XL, Ferreira TO, Huerta-Díaz MA, Partiti CSM, Souza V, Vidal-Torrado P, Macías F (2009) Geochemistry of iron and manganese in soils and sediments of a mangrove system, Island of Pai Matos (Cananeia, SP, Brazil). Geoderma 148:318–335

Portnoy JW, Giblin AE (1997) Effects of historic tidal restrictions on salt marsh sediment chemistry. Biogeochemistry 36:275–303

Postma D, Jacobsen R (1996) Redox zonation: equilibrium constraints on the Fe(III)/SO_4-reduction interface. Geochim Cosmochim Acta 60:3169–3175

Poulton SW (2003) Sulfide oxidation and iron dissolution kinetics during the reaction of dissolved sulfide with ferrihydrite. Chem Geol 202:79–94

Powell B, Martens M (2005) A review of acid sulfate soil impacts, actions and policies that impact on water quality in Great Barrier Reef catchments, including a case study on remediation at East Trinity. Mar Pollut Bull 51:149–164

Pyzik AJ, Sommer SE (1981) Sedimentary iron monosulfides: kinetics and mechanism of formation. Geochim Cosmochim Acta 45:687–698

Raiswell R, Canfield DE, Berner RA (1994) A comparison of iron extraction methods for the determination of degree of pyritisation and the recognition of iron-limited pyrite formation. Chem Geol 111:101–110

Rayment GE, Higginson FR (1992) Australian laboratory handbook of soil and water chemical methods. Inkata Press, Melbourne

Rickard DT (1974) Kinetics and mechanism of the sulfidation of goethite. Am J Sci 274:941–952

Rickard DT (1975) Kinetics and mechanism of pyrite formation at low temperatures. Am J Sci 275:636–652

Rickard D (1997) Kinetics of pyrite formation by the H_2S oxidation of iron(II) monosulfide in aqueous solutions between 25 and 125°C: the rate equation. Geochim Cosmochim Acta 61:115–134

Rickard D, Morse JW (2005) Acid volatile sulfide (AVS). Mar Chem 97:141–197

Sammut J, White I, Melville MD (1996) Acidification of an estuarine tributary in eastern Australia due to drainage of acid sulphate soils. Mar Freshw Res 47:669–684

Smith CD, Martens MA, Ahern CR, Eldershaw VJ, Powell B, Hopgood GL, Barry EV, Watling KM (2003) Demonstration of management and rehabilitation of acid sulfate soils at East Trinity: Technical Report QNRM03059. Queensland Department of Natural Resources & Mines, Indooroopilly

Soil Survey Staff (2006) Keys to soil taxonomy. US Department of Agriculture (USDA) & National Resources Conservation Service (NRCS), Washington, DC

Solomon S, Qin D, Manning M, Chen Z, Marquis M, Avery KB, Tignor M, Miller HL (eds) (2007) Climate change 2007: the physical science basis. Contribution of working group I to the fourth assessment report of the intergovernmental panel on climate change. Cambridge University Press, New York

Sullivan LA, Bush RT (2004) Iron precipitate accumulations associated with waterways in drained coastal acid sulfate landscapes of eastern Australia. Mar Freshw Res 55:1–10

Sundström R, Åström M, Österholm P (2002) Comparison of the metal content in acid sulfate soil runoff and industrial effluents in Finland. Environ Sci Technol 36:4269–4272

Tenderholt A, Hedman B, Hodgson KO (2006) PySpline: a modern, cross-platform program for the processing of raw averaged XAS edge and EXAFS data. SLAC-PUB-12219

Thode-Andersen S, Jørgensen BB (1989) Sulfate reduction and the formation of ^{35}S-labelled FeS, FeS_2, and S^0 in coastal marine sediments. Limnol Oceanogr 34:793–806

van Breemen N (1973) Soil forming processes in acid sulphate soils. In: Dost H (ed) Proceedings of the international symposium on acid sulphate soils. ILRI Publication 18, vol 1. International Institute for Land Reclamation & Improvement, Wageningen, pp 66–129

Wallmann K, Hennies K, König I, Petersen W, Knauth HD (1993) New procedure for determining reactive Fe(III) and Fe(II) minerals in sediments. Limnol Oceanogr 38:1803–1812

Yao WS, Millero FJ (1996) Oxidation of hydrogen sulfide by hydrous Fe(III) oxides in seawater. Mar Chem 52:1–16